The detection of atmospheric rivers in atmospheric reanalyses and their links to British winter floods and the large-scale climatic circulation

David A. Lavers,[1,2] Gabriele Villarini,[3,4,5] Richard P. Allan,[1,6] Eric F. Wood,[3] and Andrew J. Wade[2,7]

Received 29 April 2012; revised 12 September 2012; accepted 15 September 2012; published 19 October 2012.

[1] Atmospheric Rivers (ARs), narrow plumes of enhanced moisture transport in the lower troposphere, are a key synoptic feature behind winter flooding in midlatitude regions. This article develops an algorithm which uses the spatial and temporal extent of the vertically integrated horizontal water vapor transport for the detection of persistent ARs (lasting 18 h or longer) in five atmospheric reanalysis products. Applying the algorithm to the different reanalyses in the vicinity of Great Britain during the winter half-years of 1980–2010 (31 years) demonstrates generally good agreement of AR occurrence between the products. The relationship between persistent AR occurrences and winter floods is demonstrated using winter peaks-over-threshold (POT) floods (with on average one flood peak per winter). In the nine study basins, the number of winter POT-1 floods associated with persistent ARs ranged from approximately 40 to 80%. A Poisson regression model was used to describe the relationship between the number of ARs in the winter half-years and the large-scale climate variability. A significant negative dependence was found between AR totals and the Scandinavian Pattern (SCP), with a greater frequency of ARs associated with lower SCP values.

Citation: Lavers, D. A., G. Villarini, R. P. Allan, E. F. Wood, and A. J. Wade (2012), The detection of atmospheric rivers in atmospheric reanalyses and their links to British winter floods and the large-scale climatic circulation, *J. Geophys. Res.*, *117*, D20106, doi:10.1029/2012JD018027.

1. Introduction

[2] Atmospheric Rivers (ARs) are increasingly recognized as the cause of heavy precipitation and flooding over mid-latitude landmasses [e.g., *Ralph et al.*, 2006; *Lavers et al.*, 2011; *Neiman et al.*, 2011; *Viale and Nunez*, 2011]. These narrow plumes of enhanced moisture transport occur in the lower troposphere in the low-level jet region (within the warm sector) of extra-tropical cyclones and typically form a subsection of the broader warm conveyor belt (WCB). Heavy rainfall can result especially when ARs make landfall because of the convergence and thus vertical uplift within an AR, and most significantly when the moisture-laden air is forced to rise over mountains. Despite the negative economic and societal impacts of flooding, the atmospheric moisture ARs transport and deliver is also essential for water resources and supply [*Dettinger et al.*, 2011].

[3] Knowledge about the narrow AR region of moisture transport within extra-tropical cyclones has existed for a considerable time [e.g., *Browning and Pardoe*, 1973] and has been the subject of previous research over the Pacific Ocean [*Ralph et al.*, 2004, 2005; *Bao et al.*, 2006; *Neiman et al.*, 2008a, 2008b] and Atlantic Ocean [*Stohl et al.*, 2008; *Knippertz and Wernli*, 2010]. The connection between ARs and midlatitude heavy precipitation and flooding has been identified in western North America [*Ralph et al.*, 2006; *Neiman et al.*, 2011], and more recently in other regions including Britain [*Lavers et al.*, 2011], Tennessee, USA [*Moore et al.*, 2012] and South America [*Viale and Nunez*, 2011]. In particular, *Lavers et al.* [2011] showed that the ten largest winter floods from 1970 to 2010 in a range of British basins were associated with ARs, and that the impact was in western Britain because of the general predominance of impermeable rock and upland terrain.

[4] Broadly speaking, two approaches are generally used for the detection of ARs. The first method is to start with the atmosphere. Here the most common techniques to identify

[1]Department of Meteorology, University of Reading, Reading, UK.
[2]Walker Institute, University of Reading, Reading, UK.
[3]Department of Civil and Environmental Engineering, Princeton University, Princeton, New Jersey, USA.
[4]Willis Research Network, London, UK.
[5]Now at IIHR-Hydroscience & Engineering, University of Iowa, Iowa City, Iowa, USA.
[6]National Centre for Atmospheric Science, University of Reading, Reading, UK.
[7]Department of Geography and Environmental Science, University of Reading, Reading, UK.

Corresponding author: D. A. Lavers, Department of Meteorology, University of Reading, Earley Gate, Reading RG6 6AR, UK. (d.a.lavers@reading.ac.uk)

0148-0227/12/2012JD018027

ARs have been to evaluate the Integrated Water Vapor (IWV) in the atmosphere via satellite measurements [*Ralph et al.*, 2004; *Neiman et al.*, 2008b; *Guan et al.*, 2010], or to calculate the vertically integrated horizontal water vapor transport (hereafter, integrated vapor transport, IVT) between 1000 hPa and 300 hPa, using atmospheric reanalysis data [*Zhu and Newell*, 1998; *Roberge et al.*, 2009; *Jiang and Deng*, 2011]. For example, *Roberge et al.* [2009] considered significant poleward moisture transport (and thus AR occurrence) when the standardized IVT was greater than two standard deviations above the mean for one day. Another AR detection method using IWV and daily wind speeds and directions at 925 hPa was proposed by *Neiman et al.* [2009] and was subsequently applied to reanalysis data and climate model projections to study ARs making landfall in California [*Dettinger*, 2011]. The second approach focuses on the hydrologic impacts of these events. The first step is to identify extremes in hydrological variables, such as extreme precipitation or floods [*Ralph et al.*, 2006; *Lavers et al.*, 2011; *Neiman et al.*, 2011]. To determine if an AR was the cause of the flooding, the atmospheric state (IWV/IVT/specific humidity and wind fields) preceding the heavy precipitation and /flood events is analyzed. While the identification of the ARs driven by the hydrology is a valuable approach to improve our understanding of the hydrometeorological processes, it is not suitable to determine possible changes in ARs in a projected warmer climate because of the need to simulate cause then effect.

[5] Flooding has significant societal and economic repercussions. At least four modeling studies suggest an intensification of extremes, in particular heavy rainfall and flooding [*Voss et al.*, 2002; *Held and Soden*, 2006; *Allan and Soden*, 2008; *O'Gorman and Schneider*, 2009] and the first United Kingdom (UK) Climate Change Risk Assessment (in 2012) found that winter flooding is expected to become more commonplace in the UK, with a projected increase in flood-related damage. This work aims to determine the strength of the link between ARs and winter floods in Britain as a basis for future assessments of the impacts of climate variability on floods. To achieve this aim there were three objectives: (1) to introduce an AR detection algorithm, based on IVT calculation using gridded atmospheric data sets; (2) to compare the detected ARs with winter flood occurrence; and (3) to determine if any of the large-scale climate circulation patterns, such as the North Atlantic Oscillation or the Scandinavian pattern could explain AR occurrence in the North Atlantic.

2. Data and Methods

[6] Atmospheric reanalyses are considered to be a best estimate of the historical state of the Earth's atmosphere and are produced by assimilating meteorological/oceanic observations into Numerical Weather Prediction model output. The specific humidity q, and the zonal and meridional (u and v) wind fields for 1979–2010 were retrieved from five reanalysis products: the National Centers for Environmental Prediction (NCEP) Climate Forecast System at 0.5° × 0.5° resolution [*Saha et al.*, 2010], European Centre for Medium-Range Weather Forecasts ERA-Interim (ERAIN) at 0.7° × 0.7° resolution [*Dee et al.*, 2011], Twentieth Century Reanalysis (20CR) at 2.0° × 2.0° resolution [*Compo et al.*, 2011], National Aeronautics and Space Administration Modern Era Retrospective-Analysis for Research and Applications (MERRA) [*Rienecker et al.*, 2011] at 0.5° × 0.66° resolution and NCEP–NCAR (National Center for Atmospheric Research) at 2.5° × 2.5° resolution [*Kalnay et al.*, 1996]. The data assimilating models, analysis methods and the observations incorporated (e.g., in situ measurements and satellite data) vary between the reanalysis products resulting in differences in the reanalyses [*Rienecker et al.*, 2011; *Trenberth et al.*, 2011]. For example in terms of observations, the 20CR used an ensemble assimilation method based solely on surface pressure observations [*Compo et al.*, 2011], whereas the other four reanalyses assimilate other meteorological data sources including satellite measurements. The ERAIN, MERRA and CFSR reanalyses assimilate Special Sensor Microwave/Imager (SSM/I) water vapor channel data from 1987 resulting in a more realistic spatial simulation of water vapor over the ocean than NCEP-NCAR and 20CR (which do not assimilate SSM/I) but at the expense of inhomogeneity introduced into the time series, relating to changes in the observing system [e.g., *Trenberth et al.*, 2011; *Dee et al.*, 2011]. Visual inspection of the results from all reanalyses considered indicates that they are able to represent AR-like structures adequately. This outcome suggests that realistic sea surface temperatures and atmospheric circulation, provided by all reanalyses considered, are sufficient for simulating the large-scale structures associated with ARs. Given the differences in the reanalyses, all five are considered in this analysis.

[7] The algorithm developed to identify ARs affecting Britain calculates the IVT from 1000 hPa to 300 hPa in an Eulerian framework as follows:

$$IVT = \sqrt{\left(\frac{1}{g}\int_{1000}^{300} qu\,dp\right)^2 + \left(\frac{1}{g}\int_{1000}^{300} qv\,dp\right)^2} \qquad (1)$$

where q is the specific humidity in kg / kg, u is the zonal wind in ms^{-1}, v is the meridional wind in ms^{-1}, and g is the acceleration due to gravity.

[8] A review of past literature shows that there is not a well-established and widely applicable IVT threshold for AR occurrence. In an effort to set an IVT threshold for the study herein, the following approach was employed where the basis is to use percentiles of the IVT distribution rather than a single value, thus reflecting different IVT climatologies for different regions of the world.

[9] The same methodology was applied to each of the five reanalysis products (ERAIN is given as an example) and is based on Tables 1 and 2 in *Neiman et al.* [2008b], who identified ARs with IWV > 2 cm that impacted western North America between 32.5°N and 52.5°N during the 1998–2005 water years. A subset of these events was considered, by focusing only on the 180 ARs that occurred during the winter half-year (October to March). The IVT values (at 1200UTC for the 180 events) along the western North America coast (at the last ocean grid point) at all latitudes between 32.5°N and 52.5°N was computed, and the maximum IVT value during each of the 180 ARs retained. The median of these 180 IVT maximum values was then calculated (the vertical black line in Figure 1a shows that the

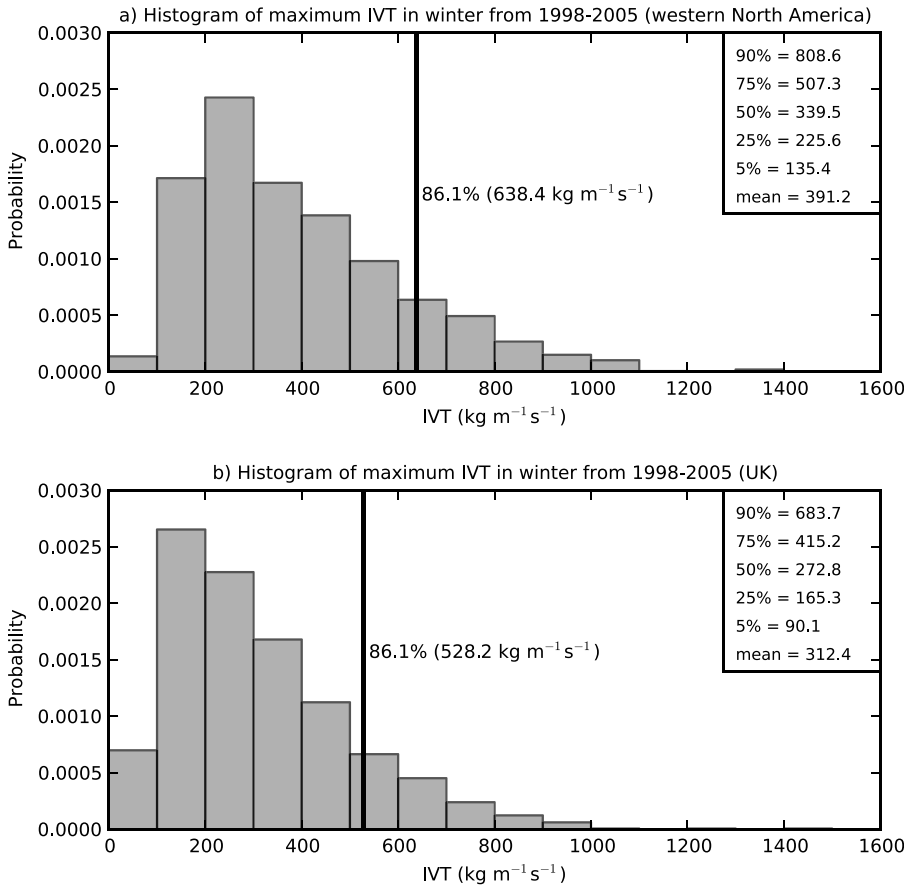

Figure 1. (a) Histogram of the maximum IVT along the western North America coast (between 32.5°N and 52.5°N) in ERA-Interim at 1200UTC on all winter days during 1998–2005. The black line represents the median IVT of the 180 winter AR events (at 1200UTC) in *Neiman et al.* [2008b]; (b) histogram of the maximum IVT along western Britain (at 4°W between 50°N and 60°N) in ERA-Interim at 1200UTC on all winter days during 1998–2005. The percentiles in the top right corners of the panels relate to the respective histograms.

median value is 638.4 kg m^{-1} s^{-1}). The percentile to which the median value (638.4 kg m^{-1} s^{-1}) corresponded in the IVT distribution calculated using the IVT values at 1200UTC on all winter half-year days during 1998–2005 was then determined; for ERAIN, it would correspond to the 86.1th percentile of the IVT distribution (Figure 1a). Finally, the IVT distribution in the region of interest (grid points spanning 50°N to 60°N along 4°W) was computed by extracting the maximum IVT on all winter half-year days (at 1200UTC) for the 1998–2005 period (Figure 1b), and the IVT value at the 86.1th percentile (528.2 kg m^{-1} s^{-1}; Figure 1b) calculated. This value was used to identify ARs affecting Britain from ERAIN. This procedure was repeated for the five reanalyses and the percentiles (IVT thresholds) were 84.4% (502.5 kg m^{-1} s^{-1}) for 20CR, 88.3% (568.2 kg m^{-1} s^{-1}) for CFSR, 86.1% (528.2 kg m^{-1} s^{-1}) for ERAIN, 87.8% (531.2 kg m^{-1} s^{-1}) for MERRA and 87.0% (548.4 kg m^{-1} s^{-1}) for NCEP-NCAR.

[10] With an IVT threshold established, the following methodology was used at each six hour time step in the five reanalysis products over the winter half-year from 1980 to 2010. The IVT was calculated at grid points spanning 50°N to 60°N along 4°W and if the maximum IVT was greater than the threshold, the grid point was retained (note that 4°W roughly corresponds to landfall in western Britain). When a grid point at 4°W was retained, the next step was to search adjacent grid points next to 4°W (to the northwest/south/southwest/west) for the highest IVT; the identified point was screened to determine if the IVT threshold was satisfied. This process was repeated *n* times across the North Atlantic where *n* is the number of reanalysis grid points along a parallel for 20° longitude (e.g., number of grid points from 4°W to 24°W at one latitude). If the IVT threshold was exceeded at the *n* points, the time step was said to have an AR affecting Britain. Since *Lavers et al.* [2011] showed that extreme winter flooding was associated with persistent AR events, only AR events that occurred for three or more time steps (18 h or more) were considered as potential flood-generating ARs (hereafter, the term AR refers to a persistent AR). Moreover, only a 4.5° latitude movement to the north or south of the initial IVT maximum at 4°W between time steps was allowed. Assuming that the mid-point of the AR (at 4°W) is given by the maximum IVT, and that ARs are of the order of 1000 km wide [*Neiman et al.*, 2008b], a 4.5° latitude movement (which is approximately equal to 500 km) means that even if the central

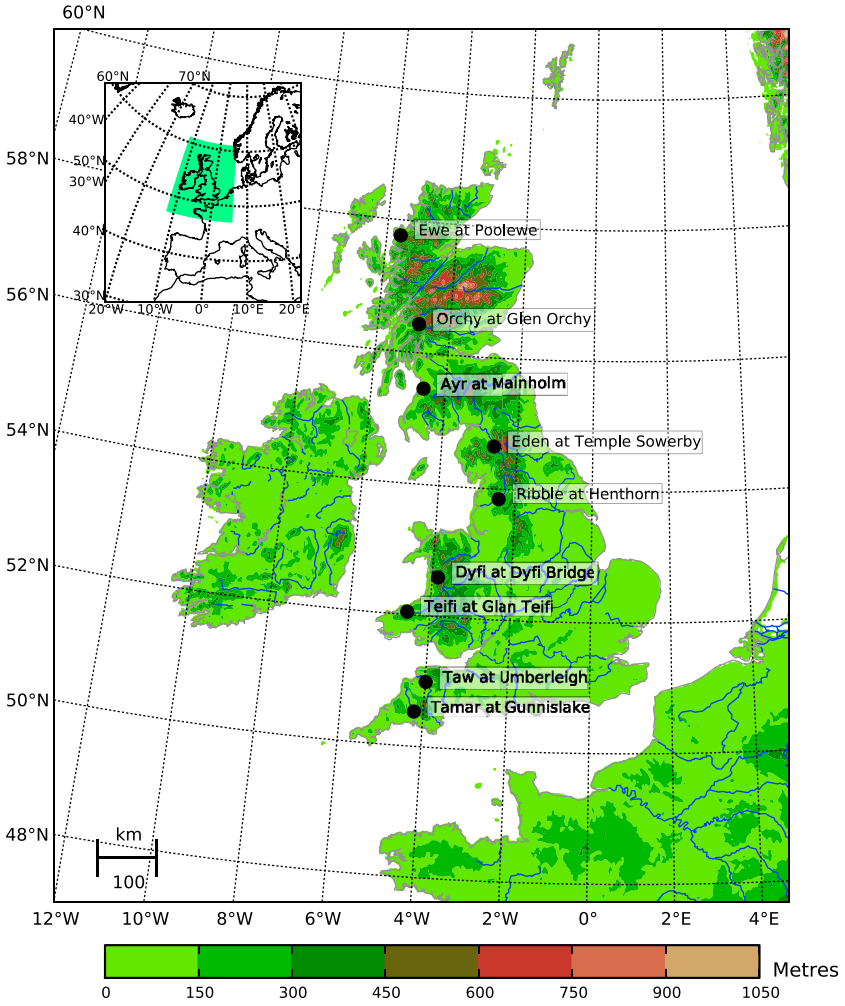

Figure 2. A map of the British Isles showing the location of the nine river basins.

location of the AR moves by 4.5°, the AR may still deliver heavy rainfall to a specific location. Furthermore, to have independent events, two AR events were considered distinct only if they were separated by more than one day.

[11] The ability of the algorithm herein to detect ARs was assessed with respect to the ARs that impacted the western North America coast between 41°N and 52.5°N in *Neiman et al.* [2008b]. The winter ARs in Table 1 in the *Neiman et al.* [2008b] database were split into a calibration (1998–2001) and a validation (2002–2005) period resulting in 47 and 56 ARs respectively. The IVT threshold was calculated for the calibration period (as the median of the maximum IVT at 1200UTC on AR days; 679.2 kg m^{-1} s^{-1}) and this was used as the threshold in the validation period. Our algorithm detected 13 ARs during 2002–2005, some of which spanned over multiple days. Of the 56 AR days in *Neiman et al.* [2008b] 18 (32.1%) were detected by our algorithm, 38 (67.9%) were not detected by our algorithm and three ARs found by the algorithm were not in the *Neiman et al.* [2008b] database. These differences with respect to *Neiman et al.* [2008b] are likely to be associated with the use of the wind field in the IVT calculation (the ARs in *Neiman et al.* [2008b] are identified using IWV) and to the fact that our algorithm has criteria for latitudinal movement and independence. Furthermore, the threshold used in our algorithm is honed to identify the most extreme ARs.

[12] Nine river basins were selected along the western seaboard of Great Britain to search for flood events that occurred after an AR made landfall (Figure 2 and Table 1). Daily river flows for the nine basins were retrieved from the UK National River Flow Archive from 1 October 1979 to 30 September 2010 (31 UK water years; the UK water year begins on 1 October). Herein, 1980 refers to the winter or water year of 1979–1980 and 2010 refers to the winter or water year of 2009–2010. The peaks-over-threshold method was used to extract on average one flood peak per winter (POT-1) over the period 1980–2010 [*Davison and Smith*, 1990; *Tallaksen et al.*, 2004]. This amounted to the 31 largest winter floods in each basin. To ensure independence of POT-1 floods, each flood had to be separated by at least seven days. Note that in the POT method some years may have more than one flood identified and some years may have no events. To associate a POT-1 flood event to a persistent AR, it was assumed that the start of an AR event occurred during the three days prior to, or on, the day of the flood. This is a reasonable assumption, considering that the nine basins generally have impermeable bedrock (as shown

Table 1. Characteristics of the Nine River Basins Obtained From the UK National River Flow Archive[a]

Basin Name	Area (km^2)	$SAAR_{61–90}$ (mm)	Median Altitude (m)	Altitude Range (m)	BHP (%)
Ewe at Poolewe	441.1	2273	310	5–1004	0
Orchy at Glen Orchy	251.2	2712	362	69–1072	0
Ayr at Mainholm	574.0	1214	212	3–592	33.6
Eden at Temple Sowerby	616.4	1146	249	92–794	4.6
Ribble at Henthorn	456.0	1348	202	39–688	0
Dyfi at Dyfi Bridge	471.3	1834	261	6–903	0
Teifi at Glan Teifi	893.6	1382	195	5–592	0
Taw at Umberleigh	826.2	1155	168	14–603	0
Tamar at Gunnislake	916.9	1216	145	8–580	0

[a]$SAAR_{61–90}$ is the standard average annual rainfall from 1961 to 1990, and BHP is the percentage of the basin underlain by high permeability bedrock.

by the low percentages of high permeability bedrock, BHP, in Table 1), allowing sufficient lag time between rainfall and the flood peak. In the Cairngorm mountains (Scotland) and on the highest mountains of western Britain (especially western Scotland) temporary snowpacks form, but low snowfall accumulation is generally expected in the majority of the area of the nine study basins because of the warm, moist westerly/southwesterly airflows in which ARs are located. Therefore the three day window between AR occurrence and a POT-1 flood is considered to be sufficient in this analysis, to capture the link between AR occurrence and the largest floods. To examine the seasonality of flood events, a block maxima approach was used over the period 1980–2010 [*Coles*, 2001; *Tallaksen et al.*, 2004]. More specifically, the maximum daily mean river flow for each winter half-year (October to March) and water year (October to September) was extracted from the flow records, generating Winter Maximum Series (WMS) and Annual Maximum Series (AMS) respectively for each of the nine basins. The half-yearly and annual blocks were used to show that the largest flood peaks in the year occur during the winter.

[13] Having identified the ARs from each of the five reanalyses, the interannual variability in their frequency was described in terms of large-scale climate variability using Poisson regression. This represents a form of Generalized Additive Model (GAM) [e.g., *Hastie and Tibshirani*, 1990], where the predictand (in this case, number of ARs per winter) can only assume discrete values and follows a Poisson distribution. If N_i is the number of ARs in winter i, then N_i is described by a conditional Poisson distribution with parameter λ_i, if

$$P\ (N_i = k|\lambda_i) = \left(\frac{e^{-\lambda_i}\lambda_i^k}{k!}\right)(\mathrm{k} = 0, 1, 2, \ldots) \qquad (2)$$

[14] The relation between the parameter and the covariates can be linear and/or nonlinear:

$$\lambda_i = \exp[\beta_0 + \beta_1 h_1(z_{1i}) + \beta_2 h_2(z_{2i}) + \cdots + \beta_n h_n(z_{ni})] \qquad (3)$$

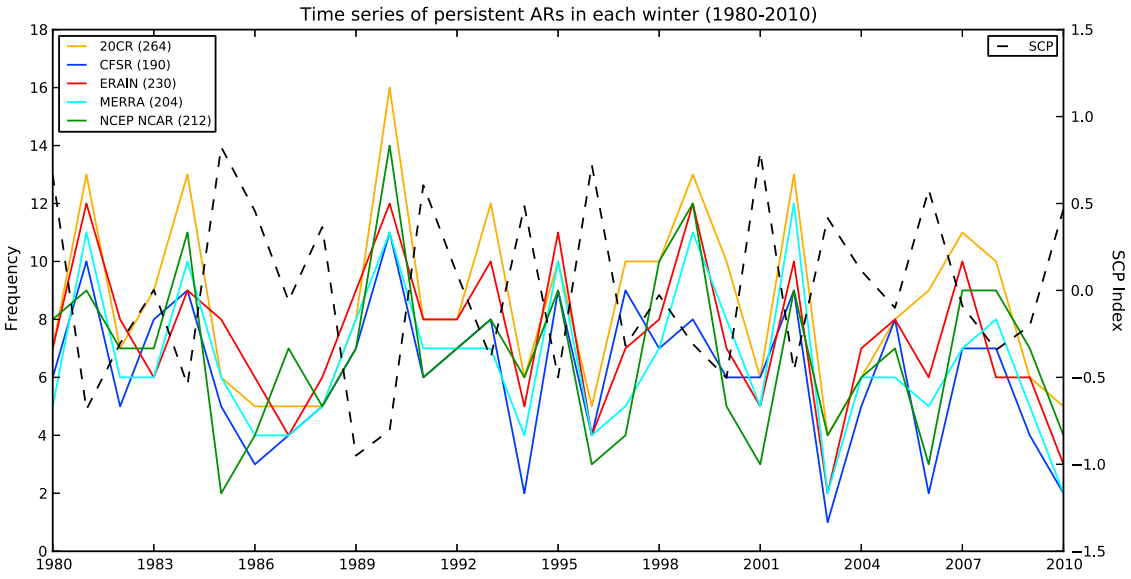

Figure 3. Time series of the number of persistent ARs in each winter half-year (October to March) over 1980–2010 in the five reanalyses (left y axis). The black dashed line represents the winter half-year Scandinavian Pattern index (anomaly values shown in the right y axis). The total number of ARs for each reanalysis product is given in the legend. Note that the year in the plots refers to the year the winter ended (e.g., "1980" refers to the 1979–1980 winter).

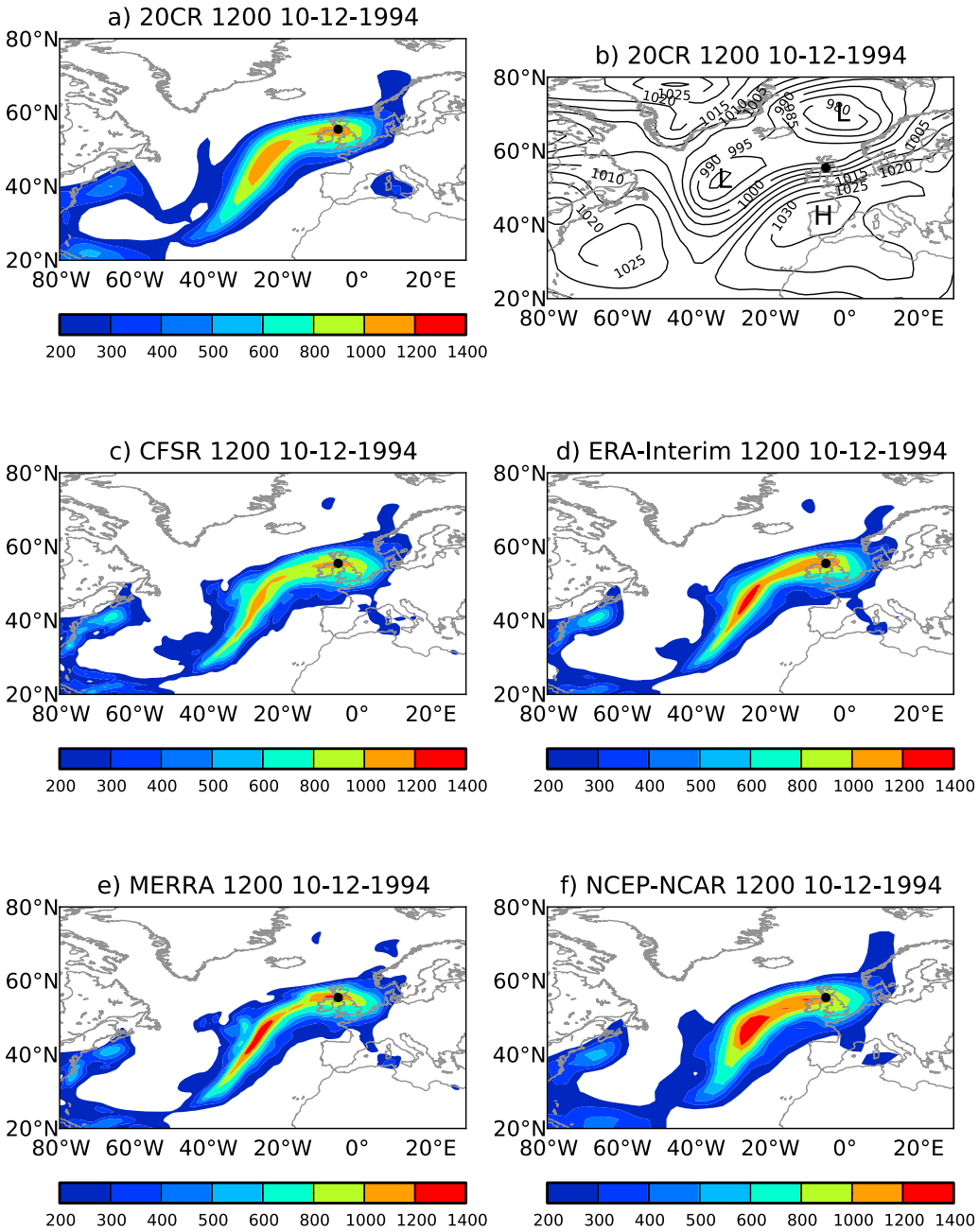

Figure 4. The IVT (in kg m^{-1} s^{-1}) for (a) 20CR, (c) CFSR, (d) ERAIN, (e) MERRA, (f) NCEP–NCAR and (b) 20CR MSLP field (in hPa) at 1200UTC 10th December 1994 before the largest flood event on 11th December 1994 in the Ayr at Mainholm basin in Scotland. Note that the color scale is in increments of 100 up to 600 kg m^{-1} s^{-1} and in increments of 200 above 600 kg m^{-1} s^{-1}. The "L" and "H" in Figure 4b refer to the Low and High pressure centers respectively; the black dots in the panels mark the location of the Ayr at Mainholm basin.

where $\{z_{1i}, z_{2i}, \ldots, z_{ni}\}$ represents a vector of n predictors for the ith year, and h_j (j = 1, …n) indicates both linear and nonlinear dependencies.

[15] If all the beta coefficients of the covariates in equation (3) are zero, then $\lambda_i = \exp(\beta_0)$, which represents a standard Poisson random variable. If the dependence between the logarithm of the rate of occurrence parameter λ_i and the predictors is linear, a Generalized Linear Model is produced (GLM) [e.g., *McCullagh and Nelder*, 1989; *Dobson*, 2001].

[16] Given the covariates, model selection was performed (both in terms of predictor selection and their functional relation to the rate of occurrence parameter of the Poisson distribution) using a stepwise approach using the Akaike Information Criterion (AIC) [*Akaike*, 1974] as the penalty criterion. This model selection procedure aims at finding a trade-off between accuracy and complexity of the model.

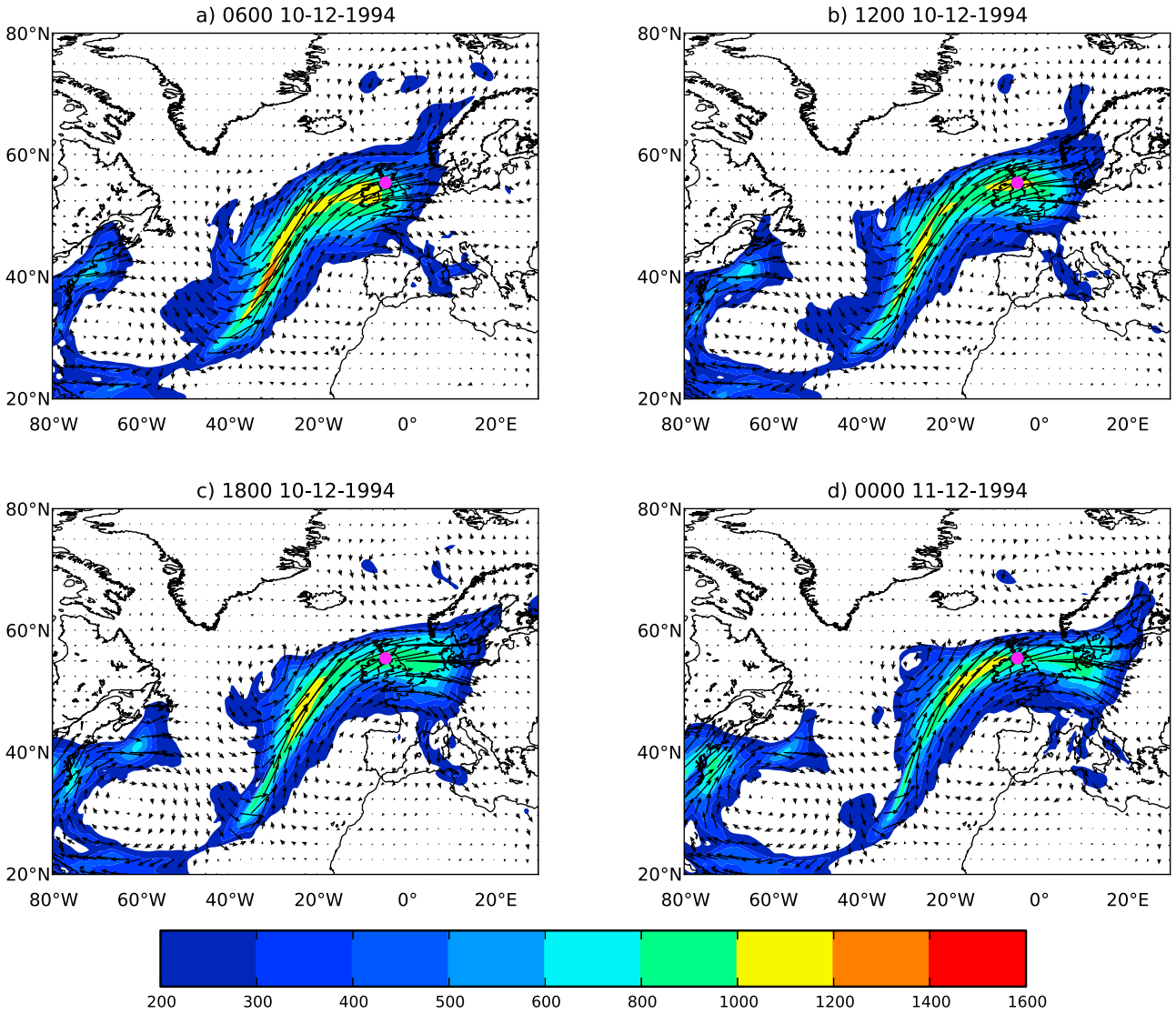

Figure 5. IVT (in kg m^{-1} s^{-1}) in the CFSR reanalysis from 0600 UTC 10th December 1994 to 0000 UTC 11th December 1994. Vectors are overlaid to show the direction of the IVT; the magenta dots in the panels mark the location of the Ayr at Mainholm basin.

The drawback is that a model with the smallest AIC does not necessarily provide information about the quality of the fit [e.g., *Hipel*, 1981]. The quality of the fit was assessed by analyzing the residuals. If the model is able to describe the systematic behavior, the residuals should be white noise. The (normalized randomized quantile) residuals [*Dunn and Smyth*, 1996] were examined by computing their first four moments (mean, variance, coefficients of skewness and kurtosis), and their Filliben correlation coefficient [*Filliben*, 1975]. The residuals plots were visually inspected using quantile-quantile and worm plots [*van Buuren and Fredriks*, 2001]. The latter are detrended forms of quantile-quantile plots, where the agreement between the selected distribution and the data is provided by the shape of the "worm." The data points should be within the 95% confidence intervals and a flat worm suggests that the data follow the selected distribution.

[17] Five climate teleconnection indices were considered as possible predictors because they were shown to be relevant to extra-tropical cyclones over Europe [*Mailier et al.*, 2006; *Vitolo et al.*, 2009]. These indices were the North Atlantic Oscillation, the east-Atlantic Pattern, the Scandinavian Pattern (SCP), the east Atlantic-western Russian Pattern and the polar-Eurasian Pattern. The monthly indices were calculated using Rotated Principal Component Analysis [*Barnston and Livezey*, 1987] and were retrieved from the Climate Prediction Center (http://www.cpc.ncep.noaa.gov/data/teledoc/telecontents.shtml). The monthly indices were averaged from October to March to obtain winter half-year index values and then used in the Poisson regression modeling framework.

3. Results and Discussion

3.1. ARs in Climate Model Reanalyses 1980–2010

[18] Time series of the number of persistent ARs in each winter half-year over 1980–2010 in the five reanalyses are shown in Figure 3. There is a large interannual variability,

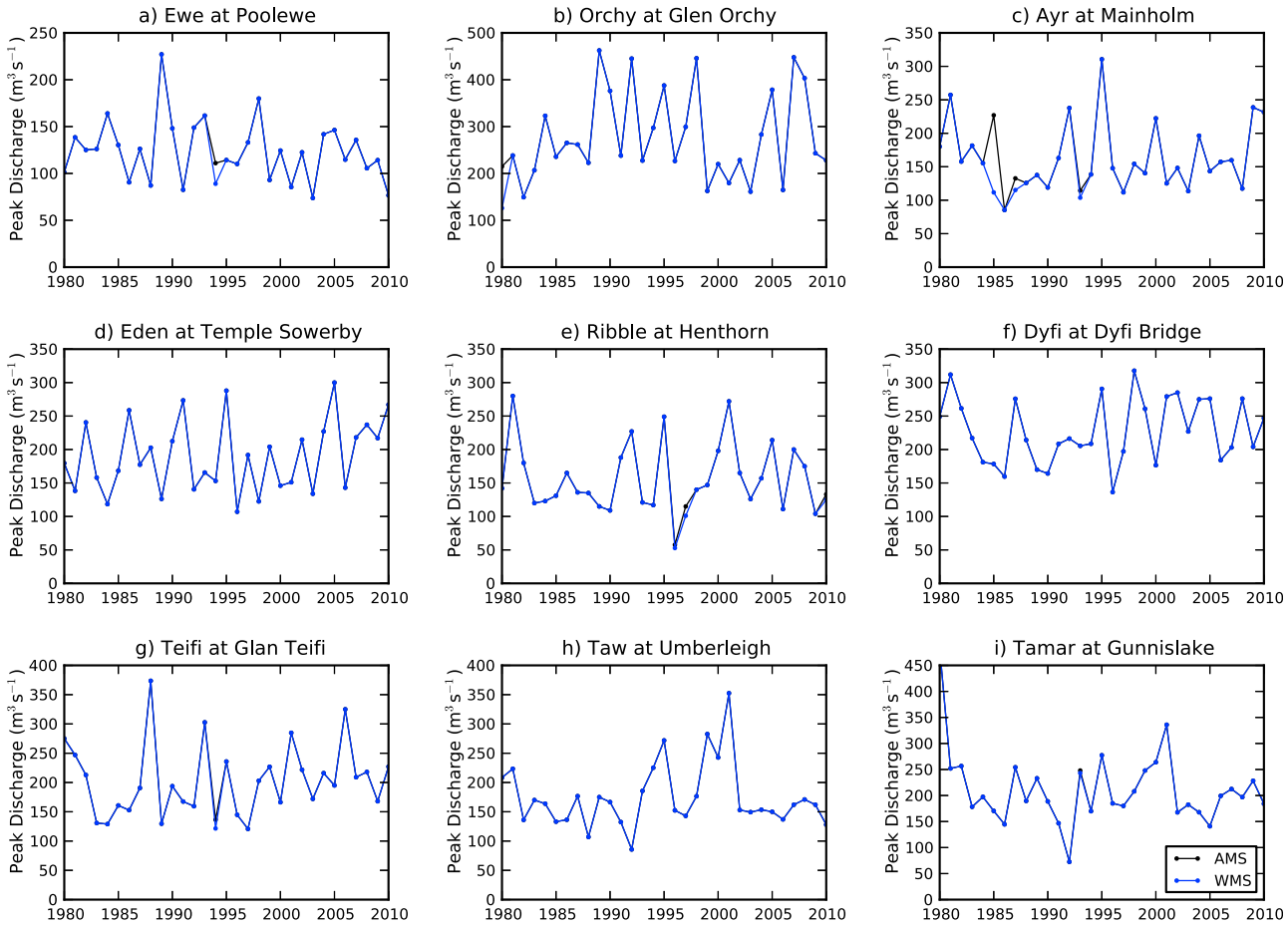

Figure 6. Time series of the Annual Maximum Series (AMS; black line) and Winter Maximum Series (WMS; blue line) for the nine study basins. The blue line is superimposed on the black line in the vast majority of the years, indicating that the annual maximum flood peaks occur during the winter.

with the number ranging from approximately 2 to 14 events per winter. Each product identifies a different number of ARs ranging from 190 in CFSR to 264 in 20CR, which may be partly due to the different IVT threshold values used for each reanalysis. There is, however, a reasonable visual agreement in the winter numbers of ARs among the products, considering the different models and data used to generate these products. It is worth noting that each reanalysis did not necessarily capture the same AR events. This is likely to be due in part, to the disparate grid resolutions which will act to locate ARs in slightly different areas. The 2010 winter had a low number of persistent ARs in the reanalysis products. Considering that a devastating flood affected Northwest England in November 2009 [*Lavers et al.*, 2011], this would suggest that an active winter in terms of persistent ARs is not necessarily a pre-requisite for large flood episodes. A single persistent AR is sufficient to cause major flooding.

[19] An example of a persistent AR detected by the algorithm is shown in the IVT fields in the five reanalyses at 1200UTC on 10th December 1994 (Figure 4). On 11th December 1994 the River Ayr at Mainholm in Scotland experienced flood conditions (310.6 $m^3 s^{-1}$; maximum daily discharge value over the period 1980–2010) and the persistent AR that led to the heavy rainfall and flood is captured well in all five reanalyses. The 20CR mean sea level pressure (MSLP) in Figure 4b shows a low pressure to the west of the British Isles that had an associated moisture transport in Figure 4a (with IVT values of about 1100 kg m^{-1} s^{-1}) in the form of an AR. The difference between ARs and WCBs noted in the Introduction in terms of their widths and moisture transport can be seen in Figure 4. The WCB can be thought of as the broad region of IVT that spans from northern France to the north of Scotland (e.g., blue region in Figure 4d), whereas the AR covers the much narrower domain over southern Scotland and northern England (e.g., orange region in Figure 4d). Although these IVT fields do not show the low-level nature of the AR or the high-altitude flow in the WCB, the enhanced moisture transport in the AR region is shown with the IVT being approximately five times larger than at the edge of the WCB. Furthermore to highlight the persistent AR behind the 11th December 1994 flood, Figure 5 shows the AR detected by the algorithm in the CFSR from 0600 10th December 1994 to 0000 11th December 1994. The continuous presence of the AR over Britain, and specifically over the Ayr basin clearly led to the heavy rainfall (101.7 mm rainfall total recorded at a local rain gauge (Garbell Burn) during the two days of the event) and subsequent flooding.

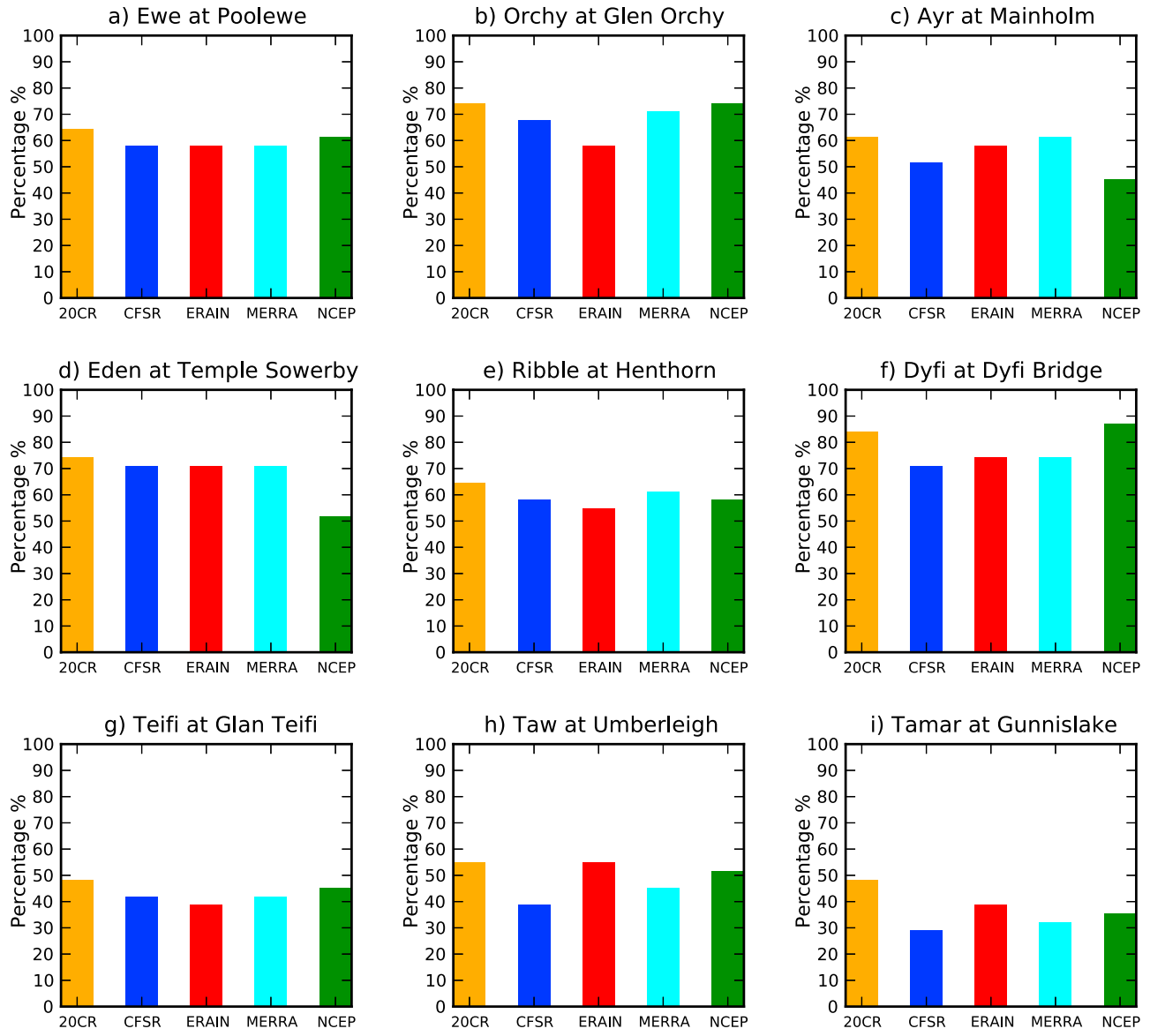

Figure 7. Percentage of the 31 POT-1 floods in each basin that are related to the persistent ARs identified in the five reanalyses.

3.2. ARs and British Winter Floods

[20] The seasonal distribution of floods is evaluated in the nine basins by using the AMS and WMS (Figure 6). In the overwhelming majority of the years and basins the winter maxima are also annual maxima suggesting that the largest flood peaks in these basins in western Britain occur during the October to March period. The hydrologic impacts of persistent ARs are assessed by identifying the percentage of the POT-1 flood peaks in each basin that are associated with

Table 2. Summary Statistics for the Poisson Modeling of AR Counts From Different Reanalysis Products[a]

	20CR	CFSR	ERAIN	MERRA	NCEP-NCAR
Intercept γ_0	2.11 (0.06)	1.77 (0.08)	1.98 (0.07)	1.84 (0.07)	1.88 (0.07)
γ_1	−0.517 (0.13)	−0.582 (0.15)	−0.449 (0.14)	−0.569 (0.15)	−0.584 (0.14)
D. of F. for the fit	2	2	2	2	2
Mean (residuals)	0.04	0.03	0.04	0.04	0.04
Variance (residuals)	0.59	0.72	0.58	0.55	0.62
Skewness (residuals)	−0.44	−0.48	−0.46	−0.29	0.09
Kurtosis(residuals)	2.18	1.99	2.56	2.26	2.54
Filliben (residuals)	0.984	0.967	0.986	0.990	0.994

[a]The logarithm of the rate of occurrence parameter is a linear function of SCP (see equation (4)). The first value is the point estimate, while the one in parentheses is the standard error; "D. of F. for the fit" indicates the degrees of freedom used for the fit.

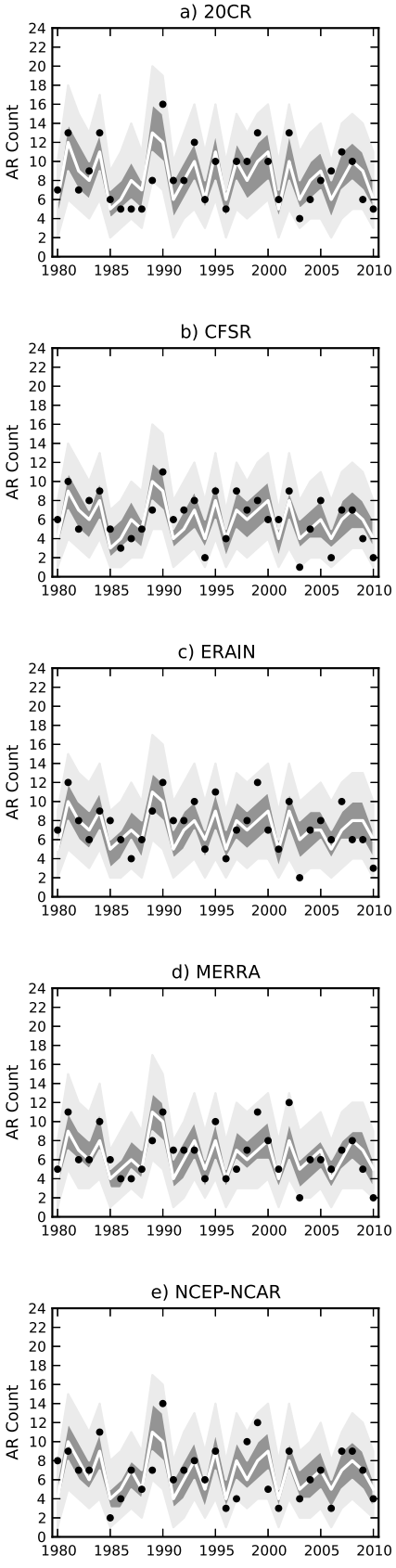

persistent ARs (Figure 7). An AR was judged as related to a flood if (1) the start of a persistent AR occurred during the three days preceding (or on the day of) the flood and (2) the average location of the AR, given by the maximum IVT at 4°W (over the AR's lifetime), was no more than 4.5° latitude away from the river basin gauging station. Figure 7 shows that ARs explain between 40 and 80% of the winter POT-1 floods occurring in nine basins in upland Britain. This result is consistent with that of *Lavers et al.* [2011].

[21] The Dyfi at Dyfi Bridge basin has the strongest AR-flood connection, with more than 70% of POT-1 floods related to a persistent AR in the five reanalyses (Figure 7f). The River Dyfi has a southwest-northeast orientation (alignment similar to the overall direction of propagation of the ARs) that favors a particularly quick rainfall-runoff response and thus strong AR-flood links. ARs are also important flood mechanisms for the other basins, with six of the nine basins (Figures 7a–7f) generally having more than 50% of the POT-1 floods occurring after a persistent AR. The lowest percentages occur in the Teifi at Glan Teifi and Tamar at Gunnislake. The Teifi and Tamar basins have water reservoirs situated in their catchment areas and therefore this water regulation could attenuate the rainfall-runoff response. It is also important, however, to highlight that there are differences across the five reanalysis products (see also Figure 3), which could be related to their different data assimilating models, analysis methods, the observations incorporated [*Rienecker et al.*, 2011] and grid resolutions.

[22] In the nine basins, the rainfall totals are high due to orographic enhancement of rainfall (as highlighted by the standard average annual rainfall from 1961 to 1990, $SAAR_{61–90}$ in Table 1) and a combination of the steep slopes (altitude range in Table 1 gives an indication of the basin slope), basin orientation and impermeable geologies (as shown by the low percentages of BHP in Table 1) cause the precipitation delivered by the ARs (and the parent extra-tropical cyclone) to be transported rapidly to the stream network causing the AR-flood connection. These results extend the previous findings on the western U.S. coast in *Ralph et al.* [2006] and *Neiman et al.* [2011] to another midlatitude location. Furthermore, as the largest flood peaks in the study basins occur during the winter, ARs therefore exert a large control on the upper tail of the flood peak distribution.

[23] To further illustrate the link between ARs and floods the number of identified persistent ARs in the five reanalyses that were related to POT-1 floods across all nine basins was calculated. The percentage of ARs related to floods for the reanalyses was 37.9% for 20CR, 44.7% for CFSR, 40.4% for ERAIN, 44.1% for MERRA and 42.0% for NCEP-NCAR. This means that on average approximately 40% of the persistent ARs captured in the reanalyses were connected with floods. These percentages could be an underestimate of

Figure 8. Modeling of the number of ARs using a Poisson regression model in which the logarithm of the rate of occurrence parameter is a linear function of the SCP. The white line represents the median (50th percentile), the dark gray region the area between the 25th and 75th percentiles, and the light gray region the area between the 5th and 95th percentiles. The black circles are the number of ARs identified in each reanalysis product.

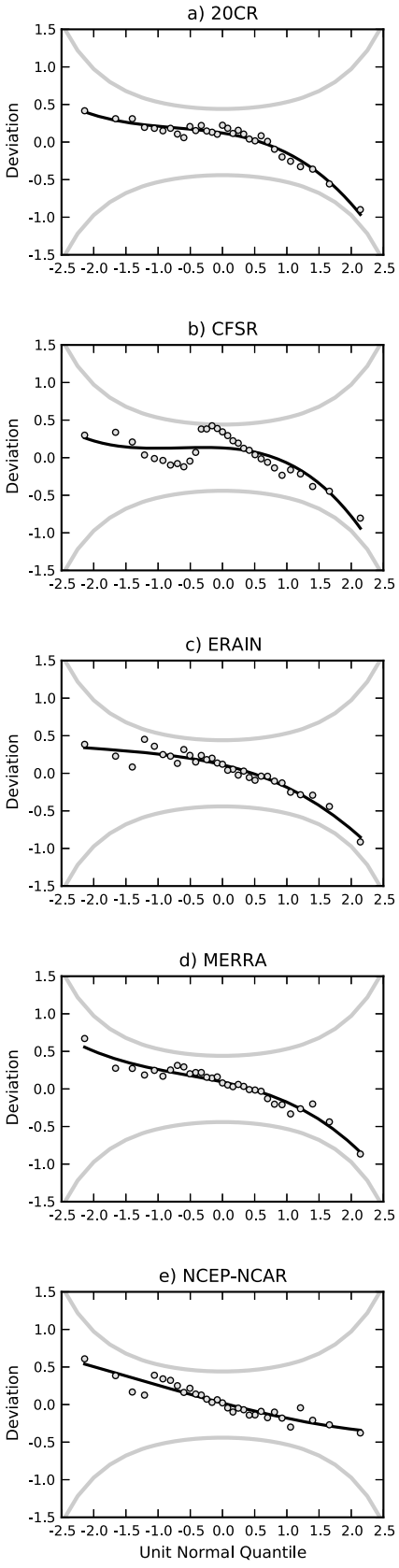

Figure 9. Worm plots for the five models in Figure 8. For a good fit, the points should be on the black line and between the two gray lines.

the flood-generating potential of ARs because of the geographical domain used (up to 60°N where no river basins are present). Note that some of the ARs cause POT-1 floods in multiple river basins.

3.3. ARs and the Large-Scale Climatic Circulation

[24] The large-scale climate circulation patterns that could be related to the occurrence of ARs were examined. Poisson regression was used to investigate the relation between the number of winter ARs and the five aforementioned climate predictors. Based on the results of the model selection, regardless of the reanalysis product the logarithm of the rate of occurrence parameter, λ for the ith year was found to be a linear function of SCP:

$$\bar{\lambda}_i = \exp[\gamma_0 + \gamma_1 SCP_i] \quad (4)$$

[25] In agreement with the results in *Mailier et al.* [2006] and *Vitolo et al.* [2009] between the number of extra-tropical cyclones and the SCP, there was a negative relation between the SCP and ARs, with a larger number of ARs associated with a more negative phase of the SCP (Table 2 and Figure 3). A positive SCP phase was shown to be associated with fewer cyclones in northern Europe, with a blocking anticyclone above northern Europe and a weak storm track located further north than usual [*Mailier et al.*, 2006]. The SCP coefficients were all statistically different from 0 at the 5% level and their values ranged from −0.449 (ERAIN) to −0.584 (NCEP-NCAR). These models were able to capture well the interannual variability exhibited by the different products (Figure 8), with large similarities (in terms of year-to-year changes and width of the percentiles of the Poisson distribution) among the different reanalysis products. The goodness of fit of these models was assessed by visual examination of the residual plots (Figure 9) and their statistics (Table 2). These diagnostics support the validity of our modeling effort, without suggesting any large problems.

4. Conclusions

[26] An AR detection algorithm, based on IVT, was developed with a threshold IVT criterion and a condition on temporal persistence and spatial location, for use in this case study of ARs and flooding in Britain. The AR detection algorithm was applied to five reanalysis products (20CR, CFSR, ERAIN, MERRA, and NCEP-NCAR) to search for ARs affecting Britain (at 4°W between 50°N and 60°N) during the winter half-years over the period 1980–2010. The results indicated that there were differences in the number of ARs detected dependent on the reanalysis product used. This is most likely due to different assimilation techniques, data, and grid resolutions.

[27] Further evidence was found that winter flooding in Britain is related to persistent AR events. This was a consistent result across the nine study basins and five reanalysis products. The percentage of winter POT-1 floods in each of the nine basins associated with ARs ranged from approximately 40 to 80%. This indicates a strong link between ARs and winter floods in Britain.

[28] Using a Poisson regression model, the frequency of persistent winter ARs was found to depend on the Scandinavian Pattern (SCP) with a significant negative

dependence between the two (larger frequency of ARs associated with lower SCP values). This was consistent across the different reanalysis products.

[29] It is proposed that three aspects require further study as a priority. The first is the impact of storm clustering. Although AR clustering is not a pre-requisite for flood occurrence (e.g., the single persistent AR responsible for the November 2009 Northwest England flood), it is possible that a flood event could follow after the quick succession of two or more persistent ARs. The second aspect is the sensitivity of the detection algorithm to the criteria used, for example the IVT threshold and AR latitudinal movement, persistence and separation in time. The final aspect is the reasons why ARs do not explain all the POT-1 floods. It is suspected that this is due to local geographical characteristics such as geological setting, land use and management, basin orientation relative to the storm tracks and temporary storage in snowpacks, reservoirs or lakes, but further research is needed to fully understand these influences.

[30] **Acknowledgments.** We thank the UK National River Flow Archive, based at the Centre for Ecology and Hydrology in Wallingford UK, for kindly providing the daily river flow data. We also thank Len Shaffrey, Benjamin Lloyd-Hughes and David Brayshaw for useful discussions that helped this paper. The work was funded by the UK Natural Environment Research Council under the Changing Water Cycle program, HydEF project (NE/I00677X/1). David Lavers is grateful to the Walker Institute Research Fund that also made the work possible, and Gabriele Villarini acknowledges financial support from the Willis Research Network. We finally acknowledge the anonymous reviewers who provided useful comments on the manuscript.

References

Akaike, H. (1974), A new look at the statistical model identification, *IEEE Trans. Autom. Control*, *19*(6), 716–723, doi:10.1109/TAC.1974.1100705.

Allan, R. P., and B. J. Soden (2008), Atmospheric warming and the amplification of precipitation extremes, *Science*, *321*(5895), 1481–1484, doi:10.1126/science.1160787.

Bao, J. W., S. A. Michelson, P. J. Neiman, F. M. Ralph, and J. M. Wilczak (2006), Interpretation of enhanced integrated water vapor bands associated with extratropical cyclones: Their formation and connection to tropical moisture, *Mon. Weather Rev.*, *134*(4), 1063–1080, doi:10.1175/MWR3123.1.

Barnston, A. G., and R. E. Livezey (1987), Classification, seasonality and persistence of low-frequency atmospheric circulation patterns, *Mon. Weather Rev.*, *115*(6), 1083–1126, doi:10.1175/1520-0493(1987)115<1083:CSAPOL>2.0.CO;2.

Browning, K. A., and C. W. Pardoe (1973), Structure of low-level jet streams ahead of mid-latitude cold fronts, *Q. J. R. Meteorol. Soc.*, *99*(422), 619–638, doi:10.1002/qj.49709942204.

Coles, S. (2001), *An Introduction to Statistical Modeling of Extreme Values*, Springer, New York.

Compo, G. P., et al. (2011), The Twentieth Century Reanalysis Project, *Q. J. R. Meteorol. Soc.*, *137*(654), 1–28, doi:10.1002/qj.776.

Davison, A. C., and R. L. Smith (1990), Models for exceedances over high thresholds, *J. R. Stat. Soc., Ser. B*, *52*, 393–442.

Dee, D. P., et al. (2011), The ERA-Interim reanalysis: Configuration and performance of the data assimilation system, *Q. J. R. Meteorol. Soc.*, *137*(656), 553–597, doi:10.1002/qj.828.

Dettinger, M. (2011), Climate change, atmospheric rivers, and floods in California - A multimodel analysis of storm frequency and magnitude changes, *J. Am. Water Resour. Assoc.*, *47*(3), 514–523, doi:10.1111/j.1752-1688.2011.00546.x.

Dettinger, M. D., F. M. Ralph, T. Das, P. J. Neiman, and D. R. Cayan (2011), Atmospheric rivers, floods and the water resources of California, *Water*, *3*, 445–478, doi:10.3390/w3020445.

Dobson, A. J. (2001), *An Introduction to Generalized Linear Models*, 2nd ed., 240 pp., CRC, Boca Raton, Fla., doi:10.1201/9781420057683.

Dunn, P. K., and G. K. Smyth (1996), Randomized quantile residuals, *J. Comput. Graph. Stat.*, *5*(3), 236–244.

Filliben, J. J. (1975), Probability plot correlation coefficient test for normality, *Technometrics*, *17*(1), 111–117, doi:10.1080/00401706.1975.10489279.

Guan, B., N. P. Molotch, D. E. Waliser, E. J. Fetzer, and P. J. Neiman (2010), Extreme snowfall events linked to atmospheric rivers and surface air temperature via satellite measurements, *Geophys. Res. Lett.*, *37*, L20401, doi:10.1029/2010GL044696.

Hastie, T. J., and R. J. Tibshirani (1990), *Generalized Additive Models*, 335 pp., Chapman and Hall, Boca Raton, Fla.

Held, I. M., and B. J. Soden (2006), Robust responses of the hydrological cycle to global warming, *J. Clim.*, *19*(21), 5686–5699, doi:10.1175/JCLI3990.1.

Hipel, K. W. (1981), Geophysical model discrimination using the Akaike information criterion, *IEEE Trans. Autom. Control*, *26*(2), 358–378, doi:10.1109/TAC.1981.1102597.

Jiang, T., and Y. Deng (2011), Downstream modulation of North Pacific atmospheric river activity by East Asian cold surges, *Geophys. Res. Lett.*, *38*, L20807, doi:10.1029/2011GL049462.

Kalnay, E., et al. (1996), The NCEP/NCAR 40-year reanalysis project, *Bull. Am. Meteorol. Soc.*, *77*(3), 437–471, doi:10.1175/1520-0477(1996)077<0437:TNYRP>2.0.CO;2.

Knippertz, P., and H. Wernli (2010), A Lagrangian climatology of tropical moisture exports to the Northern Hemispheric extratropics, *J. Clim.*, *23*(4), 987–1003, doi:10.1175/2009JCLI3333.1.

Lavers, D. A., R. P. Allan, E. F. Wood, G. Villarini, D. J. Brayshaw, and A. J. Wade (2011), Winter floods in Britain are connected to atmospheric rivers, *Geophys. Res. Lett.*, *38*, L23803, doi:10.1029/2011GL049783.

Mailier, P. J., D. B. Stephenson, C. A. T. Ferro, and K. I. Hodges (2006), Serial clustering of extratropical cyclones, *Mon. Weather Rev.*, *134*(8), 2224–2240, doi:10.1175/MWR3160.1.

McCullagh, P., and J. A. Nelder (1989), *Generalized Linear Model*, 2nd ed., 592 pp., CRC, Boca Raton, Fla.

Moore, B. J., P. J. Neiman, F. M. Ralph, and F. E. Barthold (2012), Physical processes associated with heavy flooding rainfall in Nashville, Tennessee, and vicinity during 1–2 May 2010: The role of an atmospheric river and mesoscale convective systems, *Mon. Weather Rev.*, *140*(2), 358–378, doi:10.1175/MWR-D-11-00126.1.

Neiman, P. J., et al. (2008a), Diagnosis of an intense atmospheric river impacting the Pacific Northwest: Storm summary and offshore vertical structure observed with COSMIC satellite retrievals, *Mon. Weather Rev.*, *136*(11), 4398–4420, doi:10.1175/2008MWR2550.1.

Neiman, P. J., F. M. Ralph, G. A. Wick, J. D. Lundquist, and M. D. Dettinger (2008b), Meteorological characteristics and overland precipitation impacts of atmospheric rivers affecting the West Coast of North America based on eight years of SSM/I satellite observations, *J. Hydrometeorol.*, *9*(1), 22–47, doi:10.1175/2007JHM855.1.

Neiman, P. J., A. B. White, F. M. Ralph, D. J. Gottas, and S. I. Gutman (2009), A water vapour flux tool for precipitation forecasting, *Proc. Inst. Civ. Eng. Water Manage.*, *162*(2), 83–94.

Neiman, P. J., L. J. Schick, F. M. Ralph, M. Hughes, and G. A. Wick (2011), Flooding in western Washington: The connection to atmospheric rivers, *J. Hydrometeorol.*, *12*(6), 1337–1358, doi:10.1175/2011JHM1358.1.

O'Gorman, P. A., and T. Schneider (2009), The physical basis for increases in precipitation extremes in simulations of 21st-century climate change, *Proc. Natl. Acad. Sci. U. S. A.*, *106*(35), 14,773–14,777, doi:10.1073/pnas.0907610106.

Ralph, F. M., P. J. Neiman, and G. A. Wick (2004), Satellite and CALJET aircraft observations of atmospheric rivers over the eastern North Pacific Ocean during the winter of 1997/98, *Mon. Weather Rev.*, *132*(7), 1721–1745, doi:10.1175/1520-0493(2004)132<1721:SACAOO>2.0.CO;2.

Ralph, F. M., P. J. Neiman, and R. Rotunno (2005), Dropsonde observations in low-level jets over the northeastern Pacific Ocean from CALJET-1998 and PACJET-2001: Mean vertical-profile and atmospheric-river characteristics, *Mon. Weather Rev.*, *133*(4), 889–910, doi:10.1175/MWR2896.1.

Ralph, F. M., P. J. Neiman, G. A. Wick, S. I. Gutman, M. D. Dettinger, D. R. Cayan, and A. B. White (2006), Flooding on California's Russian River: Role of atmospheric rivers, *Geophys. Res. Lett.*, *33*, L13801, doi:10.1029/2006GL026689.

Rienecker, M. M., et al. (2011), MERRA: NASA's Modern-Era Retrospective Analysis for Research and Applications, *J. Clim.*, *24*(14), 3624–3648, doi:10.1175/JCLI-D-11-00015.1.

Roberge, A., J. R. Gyakum, and E. H. Atallah (2009), Analysis of intense poleward water vapor transports into high latitudes of western North America, *Weather Forecast.*, *24*(6), 1732–1747, doi:10.1175/2009WAF2222198.1.

Saha, S., et al. (2010), The NCEP Climate Forecast System Reanalysis, *Bull. Am. Meteorol. Soc.*, *91*(8), 1015–1057, doi:10.1175/2010BAMS3001.1.

Stohl, A., C. Forster, and H. Sodemann (2008), Remote sources of water vapor forming precipitation on the Norwegian west coast at 60°N - A tale of hurricanes and an atmospheric river, *J. Geophys. Res.*, *113*, D05102, doi:10.1029/2007JD009006.

Tallaksen, L. M., H. Madsen, and H. Hisdal (2004), Frequency analysis, in *Hydrological Drought - Processes and Estimation Methods for Streamflow and Groundwater*, edited by L. M. Tallaksen and H. A. J. van Lanen, pp. 199–271, Elsevier, New York.

Trenberth, K. E., J. T. Fasullo, and J. Mackaro (2011), Atmospheric moisture transports from ocean to land and global energy flows in reanalyses, *J. Clim.*, *24*(18), 4907–4924, doi:10.1175/2011JCLI4171.1.

van Buuren, S., and M. Fredriks (2001), Worm plot: A simple diagnostic device for modelling growth reference curves, *Stat. Med.*, *20*, 1259–1277, doi:10.1002/sim.746.

Viale, M., and M. N. Nunez (2011), Climatology of winter orographic precipitation over the subtropical Central Andes and associated synoptic and regional characteristics, *J. Hydrometeorol.*, *12*(4), 481–507, doi:10.1175/2010JHM1284.1.

Vitolo, R., D. B. Stephenson, I. M. Cook, and K. Mitchell-Wallace (2009), Serial clustering of intense European storms, *Meteorol. Z.*, *18*(4), 411–424, doi:10.1127/0941-2948/2009/0393.

Voss, R., W. May, and E. Roeckner (2002), Enhanced resolution modeling study on anthropogenic climate change: Changes in extremes of the hydrological cycle, *Int. J. Climatol.*, *22*, 755–777, doi:10.1002/joc.757.

Zhu, Y., and R. E. Newell (1998), A proposed algorithm for moisture fluxes from atmospheric rivers, *Mon. Weather Rev.*, *126*(3), 725–735, doi:10.1175/1520-0493(1998)126<0725:APAFMF>2.0.CO;2.